UC Irvine
UC Irvine Previously Published Works

Title

Growth and Spatial Control of Murine Neural Stem Cells on Reflectin Films

Permalink

https://escholarship.org/uc/item/8tz3k8fj

Journal

ACS Biomaterials Science & Engineering, 6(3)

ISSN

2373-9878

Authors

Kautz, Rylan
Phan, Long
Arulmoli, Janahan
et al.

Publication Date

2020-03-09

DOI

10.1021/acsbiomaterials.9b00824

Peer reviewed

Growth and Spatial Control of Murine Neural Stem Cells on Reflectin Films

Rylan Kautz,[†] Long Phan,[†] Janahan Arulmoli,[§,‖] Atrouli Chatterjee,[†] Justin P. Kerr,[⊥] Mahan Naeim,[§] James Long,[†] Alex Allevato,[†] Jessica E. Leal-Cruz,[†] LeAnn Le,[†] Parsa Derakhshan,[†] Francesco Tombola,[#] Lisa A. Flanagan,[§,‖,▽] and Alon A. Gorodetsky*[,†,‡]

[†]Department of Chemical Engineering and Materials Science, University of California, Irvine, 916 Engineering Tower, Irvine, California 92697, United States

[‡]Department of Chemistry, University of California, Irvine, 1102 Natural Sciences II, Irvine, California 92697, United States

[§]Department of Biomedical Engineering, University of California, Irvine, 3120 Natural Sciences II, Irvine, California 92697, United States

[‖]Sue and Bill Gross Stem Cell Research Center, University of California, Irvine, 845 Health Sciences Road, Irvine, California 92697, United States

[⊥]Department of Mechanical and Aerospace Engineering, University of California, Irvine, 4200 Engineering Gateway Building, Irvine, California 92697, United States

[#]Department of Physiology and Biophysics, University of California, Irvine, 825 Health Sciences Road, Irvine, California 92697, United States

[▽]Department of Neurology, University of California, Irvine, 200 South Manchester Avenue, Orange, California 92868, United States

Ⓢ *Supporting Information*

ABSTRACT: Stem cells have attracted significant attention due to their regenerative capabilities and their potential for the treatment of disease. Consequently, significant research effort has focused on the development of protein- and polypeptide-based materials as stem cell substrates and scaffolds. Here, we explore the ability of reflectin, a cephalopod structural protein, to support the growth of murine neural stem/progenitor cells (mNSPCs). We observe that the binding, growth, and differentiation of mNSPCs on reflectin films is comparable to that on more established protein-based materials. Moreover, we find that heparin selectively inhibits the adhesion of mNSPCs on reflectin, affording spatial control of cell growth and leading to a >30-fold change in cell density on patterned substrates. The described findings highlight the potential utility of reflectin as a stem cell culture material.

KEYWORDS: *biomaterials, cephalopods, patterning, heparin, cell adhesion*
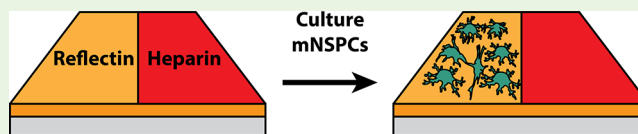
INTRODUCTION

Stem cells have historically attracted significant attention due to their regenerative capabilities and their potential for therapeutic applications.[1−9] For example, neural stem/progenitor cells (NSPCs), which are heterogeneous, self-renewing, multipotent cells capable of differentiation into neurons, astrocytes, and oligodendrocytes, have shown promise for the treatment of stroke, Parkinson's disease, and spinal cord injury in humans.[5−9] For stem cell-based treatments, the therapeutic efficacy has critically relied on influencing cellular behavior, that is, adhesion, proliferation, and differentiation, via physical and chemical cues from the surrounding environment.[10−18] Consequently, various types of materials, including proteins, peptides, polysaccharides, polymers, and ceramics, have been investigated as substrates and scaffolds for the growth of stem cells in vitro.[19−24] Among these materials, intrinsically biocompatible proteins and

polypeptides, such as collagen, fibrin, vitronectin, laminin (LAM), and fibronectin (FN), have proven especially advantageous because they not only feature motifs that can promote stem cell adhesion, proliferation, and differentiation but also can help establish environments analogous to ones found in vivo.[19−27] As such, the discovery and optimization of advantageous protein- and peptide-based substrates and scaffolds remains important in stem cell research.

For peptide- and protein-based stem cell growth materials, direct patterning represents a common strategy for controlling cellular fate and function. Therefore, several different methodologies have been developed for modifying and patterning such materials, including plasma etching, chemical functionalization,

application of electric fields, scanning probe lithography, and microcontact printing.[28−32] These methodologies have led to a better fundamental understanding of stem cell behavior and enabled applications as diverse as pharmaceutical screens, tissue engineering, neural network formation, and radiation toxicity assays.[33−36] However, when patterning peptide- and protein-based substrates, the reported approaches do feature some limitations, as they can require advanced equipment, necessitate complex multistep procedures, are often low-throughput, or have limited resolution across multiple length scales. Consequently, there exists an impetus for the continued improvement of these patterning techniques.

Recently, we have explored unique proteins called reflectins, which play a critical role in cephalopod structural coloration[37−51] as stem cell growth materials.[41] Specifically, we showed that intrinsically biocompatible reflectin films support the adhesion, proliferation, and differentiation of human neural stem/progenitor cells (hNSPCs) in a similar fashion to common neural stem cell matrix materials.[41] These efforts were motivated largely by reflectins' favorable combination of properties.[37−51] For example, reflectins can be processed into films via routine fabrication techniques, such as dip coating, drop casting, spin coating, and doctor blading.[39,42−47] In addition, these proteins can withstand relatively harsh conditions, including elevated temperature, direct metal deposition, and electrical interrogation.[44,47,49,51] Furthermore, reflectin films possess excellent electrical functionality, with bulk proton conductivities of up to ∼2.6 × 10^{-3} S cm^{-1}, thus enabling reflectin-based protonic transistors, protochromic color-changing devices, and photochemically dopable systems.[40,47−51] However, within the context of using reflectin films as stem cell growth substrates, we did not investigate NSPCs from multiple species, obtain mechanistic insight into stem cell adhesion/binding, or demonstrate direct patterning of the films.[41]

Herein, we build upon the prior work and explore the growth of murine neural stem/progenitor cells (mNSPCs) on reflectin films. First, we compare the adhesion and proliferation of mNSPCs on reflectin films and on more established protein and polypeptide scaffolds, such as FN, LAM, and poly-D-lysine. Next, we investigate and evaluate the likely mechanisms by which mNSPCs interact with reflectin. Subsequently, we demonstrate that the ability of mNSPCs to differentiate into astrocytes, neurons, and oligodendrocytes on reflectin films is comparable to that on LAM. Finally, we report the surprising observation that heparin inhibits the adhesion of mNSPCs on reflectin (presumably through electrostatic effects) and show that heparin patterning affords spatial control of mNSPC growth. Our findings underscore the potential utility of reflectin-based substrates and scaffolds for neural stem cell culture applications.

■ RESULTS AND DISCUSSION

We began our studies by fabricating reflectin films on glass substrates with the goal of using them for the growth of mNSPCs. Here we wanted to expand upon the previous finding that reflectin is an efficacious hNSPC growth material[41] and explore any species-specific effects that may arise for murine cells, which are convenient models of human disease.[52] Moreover, we selected mNSPCs that not only grow on faster time scales relative to our previously investigated hNSPCs[25] but also more efficiently differentiate into oligodendrocytes, making it possible to assess multipotent differentiation.[53]

Toward this end, we first expressed histidine-tagged *Doryteuthis (Loligo) pealeii* reflectin A1 (RfA1) variants in *E. coli* according to established protocols (Figure S1).[44,47] We then coated glass substrates with the selected reflectins via a modified doctor-blading protocol, producing films analogous to the ones previously used for the growth of hNSPCs.[41] Subsequently, we plated and cultured mNSPCs according to standard protocols, as illustrated in Figure 1A. This robust and straightforward approach facilitated the throughput of our studies with mNSPCs and enabled direct comparisons to the prior work with hNSPCs.
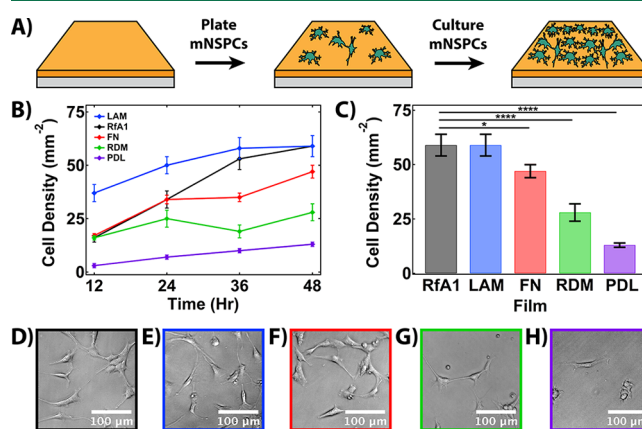

Figure 1. (A) General illustration of the procedure for the growth of mNSPCs on RfA1 films. (B) Plot of the mNSPC density on RfA1 (black), LAM (blue), FN (red), RDM (green), and PDL (purple) films as a function of time after initial plating. (C) Comparison of the mNSPC density on RfA1, LAM, FN, RDM, and PDL films after 48 h of growth. Representative phase contrast optical microscopy images of mNSPCs obtained after 48 h of growth in proliferation medium on (D) RfA1, (E) LAM, (F) FN, (G) RDM, and (H) PDL films. A one-way ANOVA with Dunnett's post hoc test was used for the statistical analysis. *$P < 0.05$, ****$P < 0.0001$. All error bars indicate the standard error of the mean from three independent experiments.

We initially evaluated the ability of films from RfA1 variants to support the adhesion and growth of mNSPCs relative to other materials that are known to support stem cells. For this purpose, we selected the commonly used extracellular matrix glycoproteins laminin (LAM) and fibronectin (FN), a mutant reflectin with a randomized amino acid sequence but overall unchanged net charge (RDM)[47] (Figure S1), and a synthetic poly-D-lysine polypeptide (PDL). To compare the adhesion and growth of mNSPCs on RfA1, LAM, FN, RDM, and PDL, we plated the cells in proliferation medium onto these materials and monitored their densities and sizes over a period of 2 days with optical microscopy (Figure 1). We anticipated that the initial observations, that is, within the first half day, would be primarily dominated by cell adhesion and that the later observations would represent a combination of cell adhesion, proliferation, and death. After 12 h, we quantified the initial adhesion and found the highest cell densities on LAM, intermediate cell densities on RfA1, FN, and RDM, and the lowest cell densities on PDL (Figure 1B). Over the next 36 h, we discovered that the cell densities were higher and quite similar to each other on RfA1 and LAM, increased but to a somewhat lesser extent on FN, changed comparatively little or not at all on RDM, and remained relatively low on PDL (Figure 1B). Specifically, after 48 h, RfA1, LAM, FN, RDM, and PDL featured cell densities of 59 ± 5, 59 ± 5, 47 ± 3, 28 ±

4, and 13 ± 1 cells/mm^2, respectively (Figure 1C). Furthermore, we noted clear morphological variability for the mNSPCs on our films, with primarily elongated morphologies and larger average surface areas that indicated healthy cell attachment on RfA1, LAM, and FN and a substantial fraction of rounded morphologies that indicated relatively poor attachment on RDM and PDL (Figure 1D−H). Indeed, after 48 h, RfA1, LAM, FN, RDM, and PDL films featured cells with average areas of 822 ± 42, 1012 ± 41, 902 ± 48, 550 ± 28, and 520 ± 22 μm^2, respectively (Figure 1D−H). Interestingly, the cell densities for RfA1 and RDM were at first comparable and then increased dramatically for the former but not for the latter with time, suggesting that the initial cell adhesion relied on the proteins' analogous net charge but that continued adhesion and growth depended on RfA1's specific amino acid sequence. Taken together, the observations demonstrated that RfA1 supported mNSPC growth in a similar fashion to the more well-established and common proteinaceous materials LAM and FN.

Because we found similar initial adhesion but significantly different subsequent growth for mNSPCs on RfA1 and RDM, we sought to gain insight into the cell surface receptors that could be responsible for the stem cells' interaction with RfA1 films. Toward this end, we assessed RNA sequencing data to quantify the relative expression of genes often associated with the binding of stem cells in different environments (Figure S2).[54,55] Specifically, we quantified the relative expression of selectins, which are transmembrane glycoproteins that mediate cellular interactions for leukocytes, platelets, and endothelial cells,[56,57] and integrins, which are heterodimeric transmembrane proteins responsible for cellular adhesion to extracellular matrices like fibronectin and laminin.[58,59] We found low levels of gene expression for the entire selectin family, that is, E-selectins, L-selectins, and P-selectins, with corresponding reads per kilobase of transcript per million reads mapped (RPKM) values of <0.1 (Figure S2). These observations indicated that selectins could not be responsible for the adhesion or growth of mNSPCs on RfA1 films. Furthermore, we found low levels of expression for the α9, β7, α3, α10, β3, α8, α4, β4, αE, α11, αL, β2, αD, αX, αM, and β6 integrins with RPKM values of ≤1, moderate levels of expression for the α5, α2, α1, and αIIb integrins with RPKM values between 1 and 10; and high levels of expression for the β1, β5, α6, β8, αV, and α7 integrins with RPKM values of ≥10 (Figure S2). Our observations indicated that only 8 out of the 24 known integrin pairs, that is, α1β1, α2β1, α5β1 α6β1, α7β1, αVβ1, αVβ5, and αVβ8, could contribute to the adhesion or growth of mNSPCs on RfA1 films, and from these pairs, α5β1, αVβ1, αVβ5, and αVβ8 are known to recognize motifs found in FN (e.g., RGD), and α1β1, α2β1, α6β1, and α7β1 are known to recognize motifs found in LAM.[60]

To better understand which of the identified integrins might facilitate the interaction of mNSPCs with reflectins, we explored how small molecules known to block cell binding on FN affected stem cell growth on RfA1 films. For this purpose, we used the synthetic peptide GRGDS, which is identical to the cell-binding motif of FN,[61] and the RGD-containing snake venom disintegrin Echistatin, which can block integrin-dependent cell adhesion on FN.[62] First, we pretreated mNSPCs with solutions containing ∼2 mM (∼1 mg/mL) GRGDS or with solutions lacking this peptide and then plated these cells on both RfA1 and FN. Then, we evaluated the resulting relative global cell densities on these

films after a period of 24 h. We found that the presence of GRGDS had little effect on the cell density on RfA1 but caused nearly an order of magnitude decrease in the cell density on FN (Figure S3). Next, we pretreated mNSPCs with solutions containing ∼2 μM (∼10 μg/mL) Echistatin or with solutions lacking this disintegrin and then plated these cells on both RfA1 and FN. We, in turn, evaluated the resulting relative global cell densities on these films after a period of 24 h. We again found that the presence of Echistatin had little effect on the cell density on RfA1 but caused more than an order of magnitude decrease in the cell density on FN (Figure S3). These observations suggested that mNSPCs were likely not interacting with RfA1 via receptors specific for RGD and that the cells may thus use other integrins for binding to RfA1.

Having observed some similarities between mNSPC growth on RfA1 and LAM, we evaluated the differentiation potential of adhered mNSPCs on these two materials. We plated mNSPCs, allowed them to reach ∼50% confluency on RfA1 or LAM, and induced differentiation by substituting proliferation medium for differentiation medium, as illustrated in Figure 2A. We then fixed the cells grown on either RfA1 or LAM, immunostained them with various markers specific for neurons, astrocytes, or oligodendrocytes (note that the nuclei were counterstained with Hoechst in all instances), and imaged the cell-covered films with fluorescence microscopy according to established protocols.[53,63−65] First, we visualized the differentiated neurons on RfA1 and LAM by staining them with antibodies that recognized cytoskeletal microtubule-associated protein 2 (MAP2) and class III β-tubulin (TuJ1). We found comparable neuron formation on both materials, with the cells displaying centralized cell bodies and elongated extended neurites (Figure 2B, left; Figure 2C, left). The calculated neuron percentages of 26.6 ± 2% for RfA1 and 25.7 ± 3% for LAM were statistically the same (Figure 2D). Next, we visualized the differentiated astrocytes on RfA1 and LAM by staining them with antibodies that recognized the intermediate filament glial fibrillary acidic protein (GFAP). We also found comparable astrocyte generation on both materials, with the cells displaying the expected morphologies and characteristic filament striations (Figure 2B, middle; Figure 2C, middle). The calculated astrocyte percentages of 16.0 ± 3% for RfA1 and 13.8 ± 2% for LAM were statistically the same (Figure 2E). In turn, we visualized the differentiated oligodendrocytes by staining them with antibodies that recognized the cell surface antigen O4. We likewise found comparable oligodendrocyte differentiation on both materials, with the cells displaying rounded cell bodies and elaborate ramified projections (Figure 2B, right; Figure 2C, right). The calculated oligodendrocyte percentages of 1.2 ± 0.6% on RfA1 and 1.7 ± 0.7% on LAM were statistically the same (Figure 2F). Here we note that less than half of the mNSPCs would be expected to differentiate into astrocytes, neurons, or oligodendrocytes under our experimental conditions, with the rest of the populations consisting of undifferentiated cells, as previously reported.[25,53,63,65] Altogether, our findings indicated that the differentiation potential of mNSPCs was almost indistinguishable on RfA1 and LAM.

While evaluating the adhesion and proliferation of mNSPCs on RfA1 and LAM, we tested and considered the effects of a variety of different media components commonly used for stem cell culture experiments (Table S1). We were surprised to discover that heparin, a glycosaminoglycan known to modulate signaling pathways via protein binding and thus to affect stem
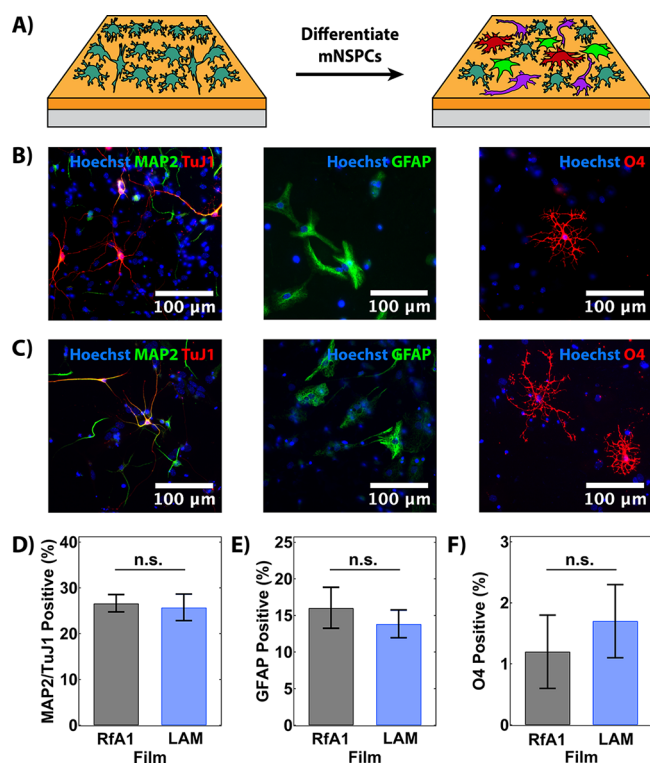
Figure 2. (A) General illustration of the differentiation of mNSPCs into neurons, astrocytes, and oligodendrocytes on RfA1 films. (B) Representative fluorescence microscopy images of RfA1 films featuring differentiated neurons coimmunostained for the cytoskeletal microtubule-associated protein MAP2 and the class III β-tubulin protein TuJ1 (left), differentiated astrocytes immunostained for the intermediate filament glial fibrillary acidic protein GFAP (middle), and differentiated oligodendrocytes immunostained for the surface antigen O4 (right). Note that the cell nuclei were stained with Hoechst in all instances. (C) Representative fluorescence microscopy images of LAM films featuring differentiated neurons coimmunostained for the cytoskeletal microtubule-associated protein MAP2 and the class III β-tubulin protein TuJ1 (left), differentiated astrocytes immunostained for the intermediate filament GFAP (middle), and differentiated oligodendrocytes immunostained for the surface antigen O4 (right). Note that the cell nuclei were stained with Hoechst in all instances. The corresponding direct comparisons of the percentage of cells that differentiated into (D) neurons, (E) astrocytes, and (F) oligodendrocytes on RfA1 (dark gray) and LAM (blue) films are shown. The error bars for neurons and astrocytes represent the standard error of the mean from three independent experiments. The error bars for oligodendrocytes represent the standard error of the mean from five independent experiments. A t test was applied for the statistical analysis, with n.s. indicating no significance. ($P < 0.05$ was considered to be statistically significant.)
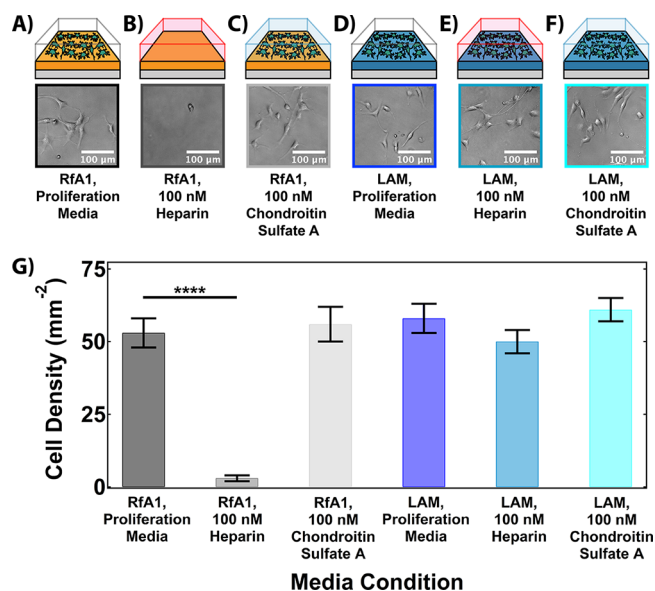

Figure 3. (A) Illustration (top) and phase contrast optical microscopy image (bottom) of mNSPCs grown on RfA1 in proliferation medium. (B) Illustration (top) and phase contrast optical microscopy image (bottom) of mNSPCs grown on RfA1 in proliferation medium supplemented with ~100 nM heparin. (C) Illustration (top) and phase contrast optical microscopy image (bottom) of mNSPCs grown on RfA1 in proliferation medium supplemented with ~100 nM chondroitin sulfate A. (D) Illustration (top) and phase contrast optical microscopy image (bottom) of mNSPCs grown on LAM in proliferation medium. (E) Illustration (top) and phase contrast optical microscopy image (bottom) of mNSPCs grown on LAM in proliferation medium supplemented with ~100 nM heparin. (F) Illustration (top) and phase contrast optical microscopy image (bottom) of mNSPCs grown on LAM in proliferation medium supplemented with ~100 nM chondroitin sulfate A. (G) Comparative plot of the mNSPC densities after 36 h of growth on RfA1 in proliferation medium (dark gray), on RfA1 in proliferation medium supplemented with ~100 nM heparin (gray), on RfA1 in proliferation medium supplemented with ~100 nM chondroitin sulfate A (light gray), on LAM in proliferation medium (blue), on LAM in proliferation medium supplemented with ~100 nM heparin (light blue), and on LAM in proliferation medium supplemented with ~100 nM heparin (cyan). Note that the optical microscopy images were obtained after 36 h of mNSPC growth. A one-way ANOVA with Dunnett's post hoc test was used for the statistical analysis. ****$P < 0.0001$. All error bars indicate the standard error of the mean from three independent experiments.

cell growth and differentiation,[66−71] appeared to substantially decrease adhesion on RfA1 but not on LAM. We therefore plated mNSPCs on these two materials and directly compared the cells' growth after a period of 36 h, in both the presence and absence of heparin (Figure 3 and Table S2). Notably, for RfA1 films in proliferation medium lacking heparin, we found that mNSPCs readily grew to high densities of 53 ± 5 cells/mm² and displayed the expected healthy elongated morphologies with surface areas of 901 ± 40 μm² (Figure 3A,G). However, for RfA1 films in proliferation medium supplemented with ~100 nM (2 μg/mL) heparin, we observed that mNSPCs exhibited little adhesion or growth, with low densities of 3 ± 1 cells/mm², and featured rounded

morphologies indicative of weak attachment, with surface areas of 549 ± 33 μm² (Figure 3B,G). In contrast, for LAM films in proliferation medium lacking heparin, we found that mNSPCs grew to densities of 58 ± 5 cells/mm² and displayed healthy cellular morphologies with surface areas of 1012 ± 46 μm² (Figure 3D,G). Likewise, for LAM films in proliferation medium supplemented with ~100 nM (2 μg/mL) heparin, we observed that mNSPCs grew to similar densities of 50 ± 4 cells/mm² and again featured healthy cellular morphologies with surface areas of 984 ± 46 μm² (Figure 3E,G). Interestingly, we discovered that heparin dramatically decreased the cell adhesion and growth on RDM and PDL but not on FN (Table S2). These findings demonstrated that heparin could serve as a potent inhibitor of mNSPC adhesion and growth specifically on positively charged materials such as RfA1 but not on negatively charged materials such as LAM.[72]

To gain further insight into the origin of heparin's influence on mNSPC growth, we assessed whether other glycosaminoglycans might likewise inhibit mNSPC adhesion on RfA1. For this purpose, we used chondroitin sulfate A because this macromolecule is known to affect neural stem cell proliferation via binding to growth factors and is chemically similar to heparin but on average has three times fewer sulfate groups per disaccharide unit.[71,73−75] We plated mNSPCs on RfA1 and LAM and compared the cells' growth after a period of 36 h, in both the presence and absence of chondroitin sulfate A (Figure 3 and Table S2). For RfA1 films in proliferation medium supplemented with ∼100 nM (2 µg/mL) chondroitin sulfate A, we found that the mNSPCs adhered and grew to densities of 56 ± 6 cells/mm^2, displaying elongated morphologies with surface areas of 830 ± 32 µm^2 (Figure 3C,G). The cells were essentially indistinguishable from ones cultured under the same conditions on RfA1 but in the absence of chondroitin sulfate A (Figure 3A,G). Similarly, for LAM films in proliferation medium supplemented with ∼100 nM (2 µg/mL) chondroitin sulfate A, we found that mNSPCs adhered and grew to densities of 61 ± 4 cells/mm^2, displaying elongated morphologies with areas of 1014 ± 40 µm^2 (Figure 3F,G). The cells were again essentially indistinguishable from ones cultured under the same conditions on LAM but in the absence of chondroitin sulfate A (Figure 3D,G). Furthermore, we observed that chondroitin sulfate A did not significantly influence cell adhesion and proliferation on RDM, PDL, and FN (Table S2). Given that some of the key differences between heparin and chondroitin sulfate A are their relative degree of sulfation and overall charge density, the totality of our findings hinted that heparin inhibited mNSPC adhesion on RfA1 (and other positively charged materials) at least in part through electrostatic effects.

Because heparin impeded mNSPC adhesion on RfA1 (but not on LAM), we investigated the possibility that this glycosaminoglycan was preferentially interacting with the surfaces of our RfA1 films. Thus we incubated RfA1 and LAM films in solutions supplemented with ∼100 nM fluorescein-labeled heparin, supplemented with ∼100 nM standard unlabeled heparin, or lacking heparin entirely. We then imaged these films, which were thoroughly washed to remove weakly bound macromolecules, with fluorescence microscopy (Figure S4). We observed the highest fluorescence intensity for RfA1 films incubated with fluorescein-labeled heparin, which was approximately three to four times greater than the background fluorescence found for RfA1 films incubated with unlabeled heparin or not incubated with heparin at all (Figure S4). We also found a lower fluorescence intensity for LAM films incubated with fluorescein-labeled heparin (relative to the analogous RfA1 films), which was comparable to the background fluorescence found for LAM films incubated with unlabeled heparin or not incubated with heparin at all (Figure S4). Taken together, these experiments revealed that heparin bound to positively charged RfA1 but not negatively charged LAM, lending additional support to the notion that this glycosaminoglycan inhibited mNSPC adhesion on some of our substrates via a charge-based mechanism.

Last, after learning that heparin was selectively binding to RfA1, we sought to leverage our discoveries for the spatial control of stem cell growth on this material. Toward this end, we dip-coated RfA1 films in solutions containing heparin, thereby leaving half of the surface pristine and modifying the other half with heparin, as illustrated in Figure 4A.
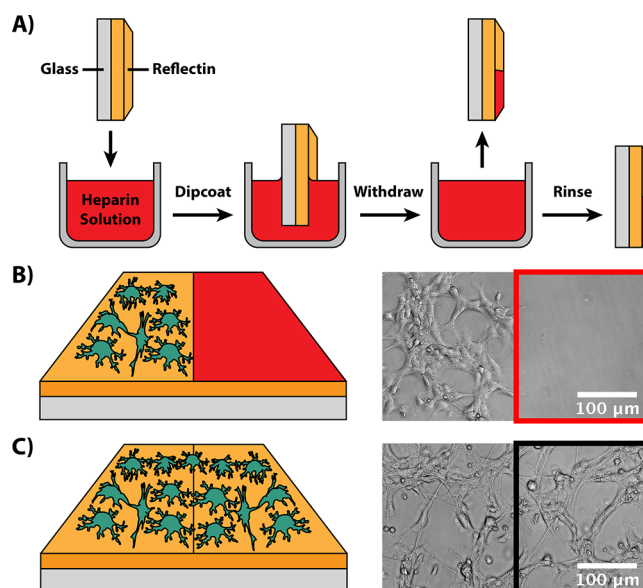

Figure 4. (A) General illustration of the dip-coating procedure for the patterning of RfA1 films with heparin. (B) Illustration (left) and phase contrast optical microscopy image (right) of an RfA1 film that was dip coated into a solution containing heparin and then used for the growth of mNSPCs. The heparin-modified area is indicated in red. (C) Illustration (left) and phase contrast optical microscopy image (right) of an RfA1 film that was dip coated into a solution lacking heparin and then used for the growth of mNSPCs. The dip-coated area is indicated in black. Note that the optical microscopy images were obtained after 24 h of mNSPC growth.

Subsequently, we plated mNSPCs at relatively high densities onto the patterned films and monitored the cell growth with optical microscopy. After a period of 24 h, we found that the films' pristine halves were covered by cells featuring typical elongated morphologies but that the heparin-modified halves featured very few adherent cells (Figure 4B). Indeed, under identical conditions, there was a >30-fold decrease in the cell density within the same film as a result of heparin patterning; essentially, the cells had chosen to adhere to the film's unmodified side (Figure 4B). For comparative purposes, we dip coated RfA1 films in solutions lacking heparin, thereby leaving both halves of their surfaces pristine and unmodified. We then plated mNSPCs at relatively high densities onto the films and again monitored the cell growth with optical microscopy. After a period of 24 h, we found that the films were completely covered with cells, observing no localization preference for either side (Figure 4C). Indeed, there was no discernible difference in the cell density or morphology on the same RfA1 film when patterning was attempted without heparin (Figure 4C). Overall, our results showed that the adsorption of heparin to RfA1 was sufficient to inhibit mNSPC adhesion and that heparin patterning could be used to direct stem cell growth on RfA1-based substrates.

CONCLUSIONS

We have comparatively investigated the growth of mNSPCs on RfA1 (relative to common protein- and peptide-based materials) and gained an improved understanding of the adhesion, proliferation, and differentiation of murine stem cells on our substrates. Initially, mNSPC adhesion on reflectin films appears to occur via electrostatic means because (1) similar or nearly identical cell densities/average areas are found on other

positively charged films, for example, RfA1 and RDM, and (2) biomolecules with a high negative charge density, that is, heparin, selectively inhibit binding on these materials. Subsequently, mNSPC growth on reflectin films is seemingly protein-sequence-dependent because (1) the cellular growth trends on RfA1, LAM, and FN are similar to each other but distinct from those on RDM and PDL and (2) the selectin family and all but four integrin pairs known to bind LAM, that is, $\alpha1\beta1$, $\alpha2\beta1$, $\alpha6\beta1$, and $\alpha7\beta1$, can be excluded as possible receptors for RfA1. Lastly, mNSPC differentiation on reflectin is comparable to the differentiation observed on other protein-based substrates because (1) indistinguishable percentages of astrocytes, neurons, and oligodendrocytes are generated on RfA1 and LAM and (2) the morphologies of the differentiated cells are comparable on RfA1 and LAM. Consequently, our observations together establish reflectin as a viable alternative to some of the most common state-of-the-art neural stem cell growth substrates and scaffolds.

The fact that heparin selectively prevents mNSPC binding on reflectin underscores our findings' potential utility within the context of neural stem cell growth. Indeed, heparin is already used both in stem cell media and in scaffolds to influence stem cell fate,[68−71] so the combination of this glycosaminoglycan and reflectin could find applications in stem cell culture protocols. For instance, given that heparin's inhibitory effect appears to be primarily electrostatic in nature (that is, due to charge neutralization), it may be possible to develop heparin-derivative-based techniques for the spatially resolved detachment of differentiated neural lineages from reflectin-based substrates. Furthermore, because patterning of RfA1 films with heparin is straightforward, robust, inexpensive, and nondestructive, our surprising findings portend favorably for the ultimate preparation of sophisticated 3D reflectin-based stem cell scaffolds. However, such future efforts will certainly necessitate a better fundamental understanding of reflectin's secondary and tertiary structures, which have not been reported to date, as well as a continued detailed exploration of the mechanisms by which stem cells interact with various reflectin isoforms.

Finally, our observations may ultimately facilitate the development of bioelectronic devices wherein reflectin serves as an active material. Previously, we have postulated that reflectin's combination of excellent biocompatibility, processability, robustness, and conductivity could enable platforms that are well suited for electrically interfacing with single neural cells.[40,76] However, the engineering and fabrication of the required device architectures would prove challenging in the absence of effective strategies for controlling cellular adhesion and localization. Thus, the findings reported herein represent another step toward cephalopod-inspired, protein-based biological electronics capable of monitoring and controlling cellular activity.

■ EXPERIMENTAL SECTION

Expression, Purification, and Characterization of Reflectin Variants. Histidine-tagged *Doryteuthis (Loligo) pealeii* reflectin A1 (RfA1) and randomized mutant reflectin A1 (RDM) proteins were prepared by following previously reported protocols.[44,47,50] In brief, the pJExpress414 expression vectors containing genes corresponding to histidine-tagged RfA1 or RDM (Figure S1) were transformed into BL21(DE3) cells (Novagen). The proteins were expressed at 37 °C using lysogeny broth (LB) (Novagen) supplemented with 100 μg/mL carbenicillin. The proteins were insoluble when expressed at 37 °C and were thus sequestered in inclusion bodies. The cells were lysed

using BugBuster (Novagen) according to manufacturer protocols, and the inclusion bodies were extracted by filtration and centrifugation. The inclusion bodies were solubilized in denaturing buffer (6 M guanidine hydrochloride) and then further purified with high-performance liquid chromatography (HPLC) on an Agilent 1260 Infinity system using a reverse-phase C18 column. For HPLC purification, the gradient was evolved from 95% Buffer A/5% Buffer B to 5% Buffer A/95% Buffer B at a flow rate of 4 mL/min over 35 min (Buffer A: 99.9% water, 0.1% trifluoroacetic acid; Buffer B: 95% acetonitrile, 4.9% water, 0.1% trifluoroacetic acid). The identities of the proteins were routinely confirmed by sodium dodecyl sulfate polyacrylamide gel electrophoresis (SDS-PAGE) and tryptic digestion, followed by mass spectrometry.

Fabrication of Protein and Polypeptide Films. Films from the reflectin variants were fabricated on glass coverslips according to established protocols.[41] In brief, the uncoated 12 mm diameter round glass coverslips (Carolina) were first cleaned sequentially with Milli-Q water, acetone, and isopropanol as well as sterilized with a bunsen burner flame. Subsequently, Teflon tape (McMaster-Carr) was applied to the edges of the coverslips to act as spacers during coating. A fresh 20 mg/mL RfA1 or RDM solution in Milli-Q water was then prepared and cast onto the coverslips in front of a plastic blade, which was translated at a constant speed across the surface at an elevated temperature to promote water evaporation and film formation. Films from the other proteins and polypeptides, that is, LAM (ThermoFisher Scientific), FN (ThermoFisher Scientific), and PDL (VWR), were prepared according to reported procedures.[53,63−65] In brief, 12 mm diameter round glass coverslips (Carolina) were incubated overnight in Minimum Essential Medium (ThermoFisher Scientific) supplemented with 20 μg/mL LAM, 10 μg/mL FN, or 40 μg/mL PDL and then thoroughly rinsed to remove any excess proteins or polypeptides. The resulting coated glass coverslips were used for cell culture and microscopy experiments as necessary.

Modification of Protein and Polypeptide Films with Glycosaminoglycans. Films from reflectin variants (that is, RfA1 and RDM) on 12 mm diameter round glass coverslips (Carolina) were modified with heparin or chondroitin sulfate A via straightforward procedures. To modify the films' entire surfaces during cell culture studies, the coated glass coverslips were cultured with mNSPCs in proliferation medium lacking glycosaminoglycans, supplemented with ~100 nM (2 μg/mL) heparin (Sigma-Aldrich), or supplemented with ~100 nM (2.8 μg/mL) chondroitin sulfate A (Sigma-Aldrich). When necessary, LAM, FN, or PDL films were immersed in solutions lacking the glycosaminoglycans, containing heparin, or containing chondroitin sulfate A under identical conditions. To modify the RfA1 or LAM films' entire surfaces for fluorescence imaging, the coated glass coverslips were incubated in differentiation medium (which did not contain growth factors that might complicate imaging) lacking any heparin, supplemented with ~100 nM (2 μg/mL) unlabeled heparin (Sigma-Aldrich), or supplemented with ~100 nM (2 μg/mL) fluorescein-labeled heparin (ThermoFisher Scientific). The substrates were subsequently thoroughly rinsed to remove any residual heparin derivatives. To modify half of the RfA1 films' surfaces, the coated glass coverslips were dipped into Dulbecco's modified Eagle's medium/Nutrient Mixture F-12 (DMEM:F12) (ThermoFisher Scientific) either lacking heparin or supplemented with ~10 μM unlabeled heparin. The substrates were subsequently gently rinsed to remove any excess heparin, taking care to avoid cross-contamination between the two sides. The resulting unmodified and heparin-modified protein films were used for cell culture and microscopy experiments as necessary.

Growth and Differentiation of Murine Neural Stem Progenitor Cells. The mNSPCs were isolated from the cerebral cortices of embryonic day 12.5 mice and passaged as nonadherent spheres at least once prior to experiments according to previously described protocols.[53] To limit the sample variability, the cortical tissue obtained from all embryos within a litter was pooled, and the isolated cells from a single litter were considered to be an independent biological replicate. For comparative adhesion and proliferation

experiments on RfA1, LAM, FN, RDM, or PDL, the mNSPCs were plated at densities of ~15 000 cells per 12 mm diameter coated coverslip. The cells were grown as adherent cultures on these substrates at 37 °C and under 5% CO_2 in proliferation medium, which consisted of DMEM:F12 (ThermoFisher Scientific), 20% (v/v) BIT 9500 (STEMCELL Technologies), 20 ng/mL epidermal growth factor (EGF) (PeproTech), and 20 ng/mL basic fibroblast growth factor (bFGF) (PeproTech) for 12 to 48 h. For some comparative adhesion and proliferation experiments on RfA1 and LAM, the proliferation medium was also supplemented with ~100 nM (2 µg/mL) heparin. For integrin inhibition experiments on RfA1 and FN, the cells were incubated in proliferation medium supplemented with ~2 mM (1 mg/mL) GRGDS (Sigma-Aldrich) or ~2 µM (10 µg/mL) Echistatin (Sigma-Aldrich) for 1 h prior to plating on the appropriate substrates. For adhesion and proliferation experiments on RfA1 films patterned with heparin via dip coating, the mNSPCs were plated at higher densities of ~100 000 cells per 12 mm diameter coated coverslip but still grown in proliferation medium lacking heparin. For differentiation experiments on RfA1 or LAM, the mNSPCs were initially plated at densities of ~40 000 cells per 12 mm diameter coated coverslip and allowed to reach ~50% confluency over ~24 h. To induce differentiation, the proliferation medium was exchanged for differentiation medium, which consisted of DMEM:F12 (Thermo-Fisher Scientific) and 20% (v/v) BIT 9500 (STEMCELL Technologies). The cells were maintained in differentiation medium for 3 days to assess neuron differentiation and for 7 days to assess astrocyte and oligodendrocyte differentiation.

Immunostaining of Murine Neural Stem Progenitor Cells Grown on Protein Films. The mNSPCs were immunostained on proteins films according to previously described protocols.[53,64,65] Initially, the differentiated mNSPCs were fixed by treatment with 4% paraformaldehyde for 10 min. The fixed cells were then treated with 0.3% Triton X-100 in PBS for 5 min and blocked with 5% bovine serum albumin (BSA) in PBS for 1 h. The cells were incubated with the following primary antibodies in PBS containing 1% BSA at 4 °C overnight: mouse anti-MAP2 IgG (1:200, 10 µg/mL, Sigma-Aldrich), rabbit anti-TuJ1 IgG (1:200, 4 µg/mL, Sigma-Aldrich), mouse anti-GFAP IgG (1:200, 134 µg/mL, Sigma-Aldrich), and mouse anti-O4 IgM (1:100, 5 µg/mL, R&D Systems). After washing, the cells were stained with the following secondary antibodies in PBS containing 1% BSA in the dark at room temperature for 2 h: donkey antimouse IgG Alexa-Fluor 488 (1:200, 10 µg/mL, ThermoFisher Scientific), donkey antirabbit IgG Alexa-Fluor 594 (1:200, 7.5 µg/mL, Jackson ImmunoResearch), and donkey antimouse IgM Alexa-Fluor 594 (1:200, 7.5 µg/mL, Jackson ImmunoResearch). Typically, the cell nuclei were also counterstained with Hoechst 33342 (ThermoFisher Scientific H3570) at a dilution of 1:1000 (2 µg/mL) in PBS at room temperature for 1 min. The resulting stained mNSPCs bound to protein films were used for all fluorescence microscopy experiments.

Optical Microscopy of Murine Neural Stem Progenitor Cells Grown on Protein and Polypeptide Films. Phase contrast optical microscopy images of mNSPCs on protein and polypeptide films were obtained by using an Advanced Microscopy Group EVOS XL microscope. As a reference, mNSPCs in suspension (rounded cells) were considered to have a ~12 µm diameter, with a ~450 µm² projection area.[77] Note that imaging was typically performed for three independent biological replicates, with one to three different substrates used per replicate and three to five randomly selected fields taken per substrate. The variance between the technical replicates was similar to or smaller than the variance between the biological replicates. To quantify the cell densities and cell areas, the images were analyzed with FIJI software.[78]

Fluorescence Microscopy of Immunostained Murine Neural Stem Progenitor Cells Grown on Protein Films. Fluorescence microscopy images of immunostained mNSPCs on protein films were obtained with a Nikon Eclipse Ti microscope and acquired with NIS element AR3.10 software. Prior to imaging, the immunolabeled mNSPCs on protein films were treated with ProLong Diamond antifade mountant (ThermoFisher Scientific). The Hoechst-stained nuclei were used to determine the total number of cells in each image.

Differentiated mNSPCs that possessed neurites with lengths at least twice those of the cell bodies and stained positive for the expression of both MAP2 and TuJ1 were classified as neurons. Differentiated mNSPCs that demonstrated the filamentous, cytoskeletal staining pattern indicative of GFAP expression were classified as astrocytes. Differentiated mNSPCs that stained positive for the surface antigen O4 were classified as oligodendrocytes. Note that imaging was typically performed for three independent biological replicates, with one to three different substrates used per replicate and three to five randomly selected fields taken per substrate. The variance between the technical replicates was similar to or smaller than the variance between the biological replicates. To quantify the cell densities and morphologies, the images were analyzed with FIJI software.[78]

RNA Sequencing of Murine Neural Stem Progenitor Cells. RNA library preparation and sequencing was performed at the UCI Genomics High Throughput Facility according to established procedures.[79] First, mNSPC RNA was isolated from suspended embryonic day 12.5 mouse cultures using a Bio-Rad RNA isolation kit (Genicity). To assess the potential genomic DNA contamination, the total RNA was reverse transcribed by using M-MLV reverse transcriptase (Promega) to generate cDNA. qRT-PCR was then performed for mouse genes 18S and Gapdh, comparing samples with and without reverse transcriptase. Genomic DNA contamination was found to be insignificant. For quality control, the total RNA was further monitored by using the Agilent Bioanalyzer Nano RNA chip and Nanodrop absorbance ratios for 260/280 and 260/230 nm. The RNA libraries were constructed according to the Illumina TruSeq stranded mRNA protocol. In brief, 250 ng of total RNA was used per sample. The mRNA in the sample was enriched using oligo dT magnetic beads and chemically fragmented for 5 min. To make cDNA, the first-strand synthesis used random primers and reverse transcriptase. After the second-strand synthesis, the double-stranded cDNA was cleaned using AMPure XP beads, the cDNA was end repaired, and the 3′ ends were adenylated. Illumina barcoded adapters were ligated on the ends, and the adapter ligated fragments were enriched by nine cycles of polymerase chain reaction (PCR). The resulting library was validated by qPCR and sized by Agilent Bioanalyzer DNA high-sensitivity chips. Separate libraries were constructed for three independent biological samples. The concentrations for the libraries were then normalized and multiplexed together. The concentration for clustering on the flowcell was 12.5 pM. The multiplexed libraries were sequenced on one lane using single-read 100-cycle chemistry for the HiSeq 2500 apparatus (version HCS 2.2.58 with real-time analysis software, RTA 1.18.64). For sequence mapping and bioinformatic analysis, the RNA-Seq data were processed as previously reported,[80] and all bioinformatics analyses were conducted by using the Galaxy platform.[81] The reads were aligned to the mouse NCBI37/mm9 reference genome with the TopHat program using primarily default parameters.[82] The alignments were restricted to unique mapping reads with two possible mismatches permitted. RPKM was calculated as described for mm9 RefSeq genes by using the SeqMonk program,[83] with mRNA RPKMs derived by counting exonic reads and dividing by the mRNA length.

Statistical Analysis. Statistical analyses were performed using Prism v.6 software (GraphPad). Data sets with two samples were compared by applying a Student's t test, and data sets containing more than two samples were analyzed by the one-way ANOVA test. A Dunnett's post hoc correction was typically applied for experiments in which multiple measurements were compared to a single control measurement.

Fluorescence Microscopy of Protein Films. Fluorescence microscopy images of RfA1 and LAM films were obtained with a Nikon Eclipse Ti microscope and acquired with NIS element AR3.10 software. Prior to imaging, the films were treated with ProLong Diamond antifade mountant (ThermoFisher Scientific). To calculate and quantify the fluorescence intensity, at least three randomly selected fields were taken per film, with the images analyzed via FIJI software.[78]

ASSOCIATED CONTENT

Ⓢ Supporting Information

The Supporting Information is available free of charge at https://pubs.acs.org/doi/10.1021/acsbiomaterials.9b00824.

Amino acid sequence for RfA1 and RDM (Figure S1); RNA sequencing data for selectin and integrin gene expression (Figure S2); relative mNSPC densities on RfA1 and FN films with and without GRGDS or Echistatin pretreatment of the cells (Figure S3); fluorescence microscopy images and relative intensities for RfA1 and LAM films incubated in differentiation medium, differentiation medium supplemented with heparin, or differentiation medium supplemented with fluorescein-labeled heparin (Figure S4); summary of the different types of media evaluated for the culturing of mNSPCs on RfA1 films (Table S1); and summary of the mNSPC densities on RfA1, LAM, FN, RDM, and PDL films in proliferation medium, proliferation medium supplemented with heparin, or proliferation medium supplemented with chondroitin sulfate A (Table S2) (PDF)

AUTHOR INFORMATION

Corresponding Author

*E-mail: alon.gorodetsky@uci.edu.

ORCID Ⓘ

Francesco Tombola: 0000-0002-9315-0352
Alon A. Gorodetsky: 0000-0002-3811-552X

Notes

The authors declare no competing financial interest.

ACKNOWLEDGMENTS

REFERENCES

(1) Gurdon, J. B. The Developmental Capacity of Nuclei Taken from Intestinal Epithelium Cells of Feeding Tadpoles. *J. Embryol. Exp. Morphol.* **1962**, *10*, 622−640.

(2) Becker, A. J.; McCulloch, E. A.; Till, J. E. Cytological Demonstration of the Clonal Nature of Spleen Colonies Derived from Transplanted Mouse Marrow Cells. *Nature* **1963**, *197*, 452−454.

(3) Siminovitch, L.; McCulloch, E. A.; Till, J. E. The Distribution of Colony-Forming Cells Among Spleen Colonies. *J. Cell. Comp. Physiol.* **1963**, *62*, 327−336.

(4) Evans, M. J.; Kaufman, M. Establishment in Culture of Pluripotential Cells from Mouse Embryos. *Nature* **1981**, *292*, 154−156.

(5) Martino, G.; Pluchino, S. The Therapeutic Potential of Neural Stem Cells. *Nat. Rev. Neurosci.* **2006**, *7*, 395−406.

(6) Kim, S. U.; de Vellis, J. Stem Cell-Based Cell Therapy in Neurological Diseases: A Review. *J. Neurosci. Res.* **2009**, *87*, 2183−2200.

(7) Daley, G. Q. The Promise and Perils of Stem Cell Therapeutics. *Cell Stem Cell* **2012**, *10*, 740−749.

(8) Trounson, A.; McDonald, C. Stem Cell Therapies in Clinical Trials: Progress and Challenges. *Cell Stem Cell* **2015**, *17*, 11−22.

(9) Madl, C. M.; Heilshorn, S. C.; Blau, H. M. Bioengineering Strategies to Accelerate Stem Cell Therapeutics. *Nature* **2018**, *557*, 335−342.

(10) Engler, A. J.; Sen, S.; Sweeney, H. L.; Discher, D. E. Matrix Elasticity Directs Stem Cell Lineage Specification. *Cell* **2006**, *126*, 677−689.

(11) Saha, K.; Keung, A. J.; Irwin, E. F.; Li, Y.; Little, L.; Schaffer, D. V.; Healy, K. E. Substrate Modulus Directs Neural Stem Cell Behavior. *Biophys. J.* **2008**, *95*, 4426−4438.

(12) Conway, A.; Schaffer, D. V. Biophysical Regulation of Stem Cell Behavior Within the Niche. *Stem Cell Res. Ther.* **2012**, *3*, 50.

(13) Ding, S.; Kingshott, P.; Thissen, H.; Pera, M.; Wang, P. Y. Modulation of Human Mesenchymal and Pluripotent Stem Cell Behavior Using Biophysical and Biochemical Cues: A Review. *Biotechnol. Bioeng.* **2017**, *114*, 260−280.

(14) Curran, J. M.; Chen, R.; Hunt, J. A. The Guidance of Human Mesenchymal Stem Cell Differentiation in Vitro by Controlled Modifications to the Cell Substrate. *Biomaterials* **2006**, *27*, 4783−4793.

(15) Das, R. K.; Zouani, O. F. A Review of the Effects of the Cell Environment Physicochemical Nanoarchitecture on Stem Cell Commitment. *Biomaterials* **2014**, *35*, 5278−5293.

(16) Murphy, W. L.; McDevitt, T. C.; Engler, A. J. Materials as Stem Cell Regulators. *Nat. Mater.* **2014**, *13*, 547−557.

(17) Dalby, M. J.; Gadegaard, N.; Oreffo, R. O. C. Harnessing Nanotopography and Integrin-Matrix Interactions to Influence Stem Cell Fate. *Nat. Mater.* **2014**, *13*, 558−569.

(18) Crowder, S. W.; Leonardo, V.; Whittaker, T.; Papathanasiou, P.; Stevens, M. M. Material Cues as Potent Regulators of Epigenetics and Stem Cell Function. *Cell Stem Cell* **2016**, *18*, 39−52.

(19) Willerth, S. M.; Sakiyama-Elbert, S. E. Combining stem cells and biomaterial scaffolds for constructing tissues and cell delivery. *StemBook* **2008**, 1.

(20) Little, L.; Healy, K. E.; Schaffer, D. V. Engineering Biomaterials for Synthetic Neural Stem Cell Microenvironments. *Chem. Rev.* **2008**, *108*, 1787−1796.

(21) Enam, S.; Jin, S. Substrates for Clinical Applicability of Stem Cells. *World Journal of Stem Cells* **2015**, *7*, 243−252.

(22) Schmidt, S.; Lilienkampf, A.; Bradley, M. New Substrates for Stem Cell Control. *Philos. Trans. R. Soc., B* **2018**, *373*, 20170223.

(23) Hagbard, L.; Cameron, K.; August, P.; Penton, C.; Parmar, M.; Hay, D. C.; Kallur, T. Developing Defined Substrates for Stem Cell Culture and Differentiation. *Philos. Trans. R. Soc., B* **2018**, *373*, 20170230.

(24) Votteler, M.; Kluger, P. J.; Walles, H.; Schenke-Layland, K. Stem Cell Microenvironments - Unveiling the Secret of How Stem Cell Fate is Defined. *Macromol. Biosci.* **2010**, *10*, 1302−1315.

(25) Flanagan, L. A.; Rebaza, L. M.; Derzic, S.; Schwartz, P. H.; Monuki, E. S. Regulation of Human Neural Precursor Cells by Laminin and Integrins. *J. Neurosci. Res.* **2006**, *83*, 845−856.

(26) Domogatskaya, A.; Rodin, S.; Tryggvason, K. Functional Diversity of Laminins. *Annu. Rev. Cell Dev. Biol.* **2012**, *28*, 523−553.

(27) Singh, P.; Schwarzbauer, J. E. Fibronectin and Stem Cell Differentiation − Lessons from Chondrogenesis. *J. Cell Sci.* **2012**, *125*, 3703−3712.

(28) Deglincerti, A.; Etoc, F.; Guerra, M. C.; Martyn, I.; Metzger, J.; Ruzo, A.; Simunovic, M.; Yoney, A.; Brivanlou, A. H.; Siggia, E.; Warmflash, A. Self-Organization of Human Embryonic Stem Cells on Micropatterns. *Nat. Protoc.* **2016**, *11*, 2223−2232.

(29) Saha, K.; Mei, Y.; Reisterer, C. M.; Pyzocha, N. K.; Yang, J.; Muffat, J.; Davies, M. C.; Alexander, M. R.; Langer, R.; Anderson, D. G.; Jaenisch, R. Surface-Engineered Substrates for Improved Human Pluripotent Stem Cell Culture Under Fully Defined Conditions. *Proc. Natl. Acad. Sci. U. S. A.* **2011**, *108*, 18714−18719.

(30) Saltó, C.; Saindon, E.; Bolin, M.; Kanciurzewska, A.; Fahlman, M.; Jager, E. W.; Tengvall, P.; Arenas, E.; Berggren, M. Control of Neural Stem Cell Adhesion and Density by an Electronic Polymer Surface Switch. *Langmuir* **2008**, *24*, 14133−14138.

(31) Giam, L. R.; Massich, M. D.; Hao, L.; Shin Wong, L.; Mader, C. C.; Mirkin, C. A. Scanning Probe-Enabled Nanocombinatorics Define the Relationship Between Fibronectin Feature Size and Stem Cell Fate. *Proc. Natl. Acad. Sci. U. S. A.* **2012**, *109*, 4377−4382.

(32) Peerani, R.; Bauwens, C.; Kumacheva, E.; Zandstra, P. W. Patterning Mouse and Human Embryonic Stem Cells Using Micro-Contact Printing. *Methods Mol. Biol.* **2009**, *482*, 21−33.

(33) Wu, M.-H.; Huang, S.-B.; Lee, G.-B. Microfluidic Cell Culture Systems for Drug Research. *Lab Chip* **2010**, *10*, 939−956.

(34) Lee, C. J.; Huie, P.; Leng, T.; Peterman, M. C.; Marmor, M. F.; Blumenkranz, M. S.; Bent, S. F.; Fishman, H. A. Microcontact Printing on Human Tissue for Retinal Cell Transplantation. *Arch. Ophthalmol.* **2002**, *120*, 1714−1718.

(35) Dermutz, H.; Grüter, R. R.; Truong, A. M.; Demko, L.; Voros, J.; Zambelli, T. Local Polymer Replacement for Neuron Patterning and in Situ Neurite Guidance. *Langmuir* **2014**, *30*, 7037−7046.

(36) Xia, J.; Qiu, Y.; Xun, X.; Ma, L.; Guan, J.; Su, M. Single Cell Patterning for High Throughput Sub-Cellular Toxicity Assay. *Anal. Chim. Acta* **2018**, *1007*, 26−32.

(37) Phan, L.; Kautz, R.; Leung, E. M.; Naughton, K. L.; Van Dyke, Y.; Gorodetsky, A. A. Dynamic Materials Inspired by Cephalopods. *Chem. Mater.* **2016**, *28*, 6804−6816.

(38) Levenson, R.; DeMartini, D. G.; Morse, D. E. Molecular Mechanisms of Reflectin's Tunable Biophotonic Control: Opportunities and Limitations for New Optoelectronics. *APL Mater.* **2017**, *5*, 104801.

(39) Chatterjee, A.; Norton-Baker, B.; Bagge, L. E.; Patel, P.; Gorodetsky, A. A. An Introduction to Color-Changing Systems from the Cephalopod Protein Reflectin. *Bioinspiration & Biomimetics* **2018**, *13*, 045001.

(40) Kautz, R.; Ordinario, D. D.; Tyagi, V.; Patel, P.; Nguyen, T. N.; Gorodetsky, A. A. Cephalopod-Derived Biopolymers for Ionic and Protonic Transistors. *Adv. Mater.* **2018**, *30*, 1704917.

(41) Phan, L.; Kautz, R.; Arulmoli, J.; Kim, I. H.; Le, D. T.; Shenk, M. A.; Pathak, M. M.; Flanagan, L. A.; Tombola, F.; Gorodetsky, A. A. Reflectin as a Material for Neural Stem Cell Growth. *ACS Appl. Mater. Interfaces* **2016**, *8*, 278−284.

(42) Kramer, R. M.; Crookes-Goodson, W. J.; Naik, R. R. The Self-Organizing Properties of Squid Reflectin Protein. *Nat. Mater.* **2007**, *6*, 533−538.

(43) Dennis, P. B.; Singh, K. M.; Vasudev, M. C.; Naik, R. R.; Crookes-Goodson, W. J. Research Update: A Minimal Region of Squid Reflectin for Vapor-Induced Light Scattering. *APL Mater.* **2017**, *5*, 120701.

(44) Phan, L.; Walkup, W. G., IV; Ordinario, D. D.; Karshalev, E.; Jocson, J.-M.; Burke, A. M.; Gorodetsky, A. A. Reconfigurable Infrared Camouflage Coatings from a Cephalopod Protein. *Adv. Mater.* **2013**, *25*, 5621−5655.

(45) Phan, L.; Ordinario, D. D.; Karshalev, E.; Walkup, W. G., IV; Shenk, M. A.; Gorodetsky, A. A. Infrared Invisibility Stickers Inspired by Cephalopods. *J. Mater. Chem. C* **2015**, *3*, 6493−6498.

(46) Naughton, K. L.; Phan, L.; Leung, E. M.; Kautz, R.; Lin, Q.; Van Dyke, Y.; Marmiroli, B.; Sartori, B.; Arvai, A.; Li, S.; Pique, M. E.; Naeim, M.; Kerr, J. P.; Aquino, M. J.; Roberts, V. A.; Getzoff, E. D.; Zhu, C.; Bernstorff, S.; Gorodetsky, A. A. Gorodetsky. Self-Assembly of the Cephalopod Protein Reflectin. *Adv. Mater.* **2016**, *28*, 8405−8412.

(47) Ordinario, D. D.; Phan, L.; Walkup, W. G., IV; Jocson, J.-M.; Karshalev, E.; Hüsken, N.; Gorodetsky, A. A. Bulk Protonic

Conductivity in a Cephalopod Structural Protein. *Nat. Chem.* **2014**, *6*, 596−602.

(48) Ordinario, D. D.; Phan, L.; Jocson, J.-M.; Nguyen, T.; Gorodetsky, A. A. Protonic Transistors from Thin Reflectin Films. *APL Mater.* **2015**, *3*, 014907.

(49) Ordinario, D. D.; Phan, L.; Van Dyke, Y.; Nguyen, T.; Smith, A. G.; Nguyen, M.; Mofid, N. M.; Dao, M. K.; Gorodetsky, A. A. Photochemical Doping of Protonic Transistors from a Cephalopod Protein. *Chem. Mater.* **2016**, *28*, 3703−3710.

(50) Ordinario, D. D.; Phan, L.; Walkup, W. G., IV; Leung, E. M.; Van Dyke, Y.; Nguyen, M.; Smith, A. G.; Kerr, J. P.; Naeim, M.; Kymissis, I.; Gorodetsky, A. A. Production and Electrical Characterization of the Reflectin A2 Isoform from Doryteuthis (Loligo) pealeii. *RSC Adv.* **2016**, *6*, 57103−57107.

(51) Ordinario, D. D.; Leung, E. M.; Phan, L.; Kautz, R.; Lee, W. K.; Naeim, M.; Kerr, J. P.; Aquino, M. J.; Sheehan, P. E.; Gorodetsky, A. A. Protochromic Devices from a Cephalopod Structural Protein. *Adv. Opt. Mater.* **2017**, *5*, 1600751.

(52) Rosenthal, N.; Brown, S. The Mouse Ascending: Perspectives for Human-Disease Models. *Nat. Cell Biol.* **2007**, *9*, 993−999.

(53) Arulmoli, J.; Pathak, M. M.; McDonnell, L. P.; Nourse, J. L.; Tombola, F.; Earthman, J. C.; Flanagan, L. A. Static Stretch Affects Neural Stem Cell Differentiation in an Extracellular Matrix-Dependent Manner. *Sci. Rep.* **2015**, *5*, 1−8.

(54) Ozsolak, F.; Milos, P. M. RNA Sequencing: Advances, Challenges and Opportunities. *Nat. Rev. Genet.* **2011**, *12*, 87−98.

(55) Yale, A. R.; Nourse, J. L.; Lee, K. R.; Ahmed, S. N.; Arulmoli, J.; Jiang, A. Y.; McDonnell, L. P.; Botten, G. A.; Lee, A. P.; Monuki, E. S.; Demetriou, M.; Flanagan, L. A. Cell Surface N-Glycans Influence Electrophysiological Properties and Fate Potential of Neural Stem Cells. *Stem Cell Rep.* **2018**, *11*, 869−882.

(56) Gumbiner, B. M. Cell Adhesion: The Molecular Basis of Tissue Architecture and Morphogenesis. *Cell* **1996**, *84*, 345−357.

(57) Alberts, B.; Johnson, A.; Lewis, J.; Raff, M.; Roberts, K.; Walter, P. Molecular Biology of the Cell. *Q. Rev. Biol.* **2003**, *78*, 91.

(58) Hynes, R. O. Integrins: Versatility, Modulation, and Signaling in Cell Adhesion. *Cell* **1992**, *69*, 11−25.

(59) Giancotti, F. G.; Ruoslahti, E. Integrin Signaling. *Science* **1999**, *285*, 1028−1032.

(60) Takada, Y.; Ye, X.; Simon, S. The Integrins. *Genome Biology* **2007**, *8*, 215.

(61) Oldberg, A.; Franzén, A.; Heinegård, D. Cloning and Sequence Analysis of Rat Bone Sialoprotein (Osteopontin) cDNA Reveals an Arg-Gly-Asp Cell-Binding Sequence. *Proc. Natl. Acad. Sci. U. S. A.* **1986**, *83*, 8819−8823.

(62) Ramos, O. H. P.; Selistre-de-Araujo, H. S. Snake Venom Metalloproteases − Structure and Function of Catalytic and Disintegrin Domains. *Comp. Biochem. Physiol., Part C: Toxicol. Pharmacol.* **2006**, *142*, 328−346.

(63) Flanagan, L. A.; Lu, J.; Wang, L.; Marchenko, S. A.; Jeon, N. L.; Lee, A. P.; Monuki, E. S. Unique Dielectric Properties Distinguish Stem Cells and their Differentiated Progeny. *Stem Cells* **2008**, *26*, 656−665.

(64) Simon, M. G.; Li, Y.; Arulmoli, J.; McDonnell, L. P.; Akil, A.; Nourse, J. L.; Lee, A. P.; Flanagan, L. A. Increasing Label-Free Stem Cell Sorting Capacity to Reach Transplantation-Scale Throughput. *Biomicrofluidics* **2014**, *8*, 064106.

(65) Nourse, J. L.; Prieto, J. L.; Dickson, A. R.; Lu, J.; Pathak, M. M.; Tombola, F.; Demetriou, M.; Lee, A. P.; Flanagan, L. A. Membrane Biophysics Define Neuron and Astrocyte Progenitors in the Neural Lineage. *Stem Cells* **2014**, *32*, 706−716.

(66) Capila, I.; Linhardt, R. J. Heparin-Protein Interactions. *Angew. Chem., Int. Ed.* **2002**, *41*, 390−412.

(67) Meneghetti, M. C.; Hughes, A. J.; Rudd, T. R.; Nader, H. B.; Powell, A. K.; Yates, E. A.; Lima, M. A. Heparan Sulfate and Heparin Interactions with Proteins. *J. R. Soc., Interface* **2015**, *12*, 20150589.

(68) Caldwell, M. A.; Svendsen, C. N. Heparin, but not Other Proteoglycans Potentiates the Mitogenic Effects of FGF-2 on Mesencephalic Precursor Cells. *Exp. Neurol.* **1998**, *152*, 1−10.

(69) Liao, L.; Shi, B.; Chang, H.; Su, X.; Zhang, L.; Bi, C.; Shuai, Y.; Du, X.; Deng, Z.; Jin, Y. Heparin Improves BMSC Cell Therapy: Anticoagulant Treatment by Heparin Improves the Safety and Therapeutic Effect of Bone Marrow-Derived Mesenchymal Stem Cell Cytotherapy. *Theranostics* **2017**, *7*, 106−116.

(70) Lei, J.; Yuan, Y.; Lyu, Z.; Wang, M.; Liu, Q.; Wang, H.; Yuan, L.; Chen, H. Deciphering the Role of Sulfonated Unit in Heparin-Mimicking Polymer to Promote Neural Differentiation of Embryonic Stem Cells. *ACS Appl. Mater. Interfaces* **2017**, *9*, 28209−28221.

(71) Pickford, C.; Holley, R.; Meade, K.; Merry, C. Glycans in Embryonic Stem Cells. *Glycans in Diseases and Therapeutics* **2011**, 113−137.

(72) Bronner-Fraser, M. Latex Beads as Probes of a Neural Crest Pathway: Effects of Laminin, Collagen, and Surface Charge on Bead Translocation. *J. Cell Biol.* **1984**, *98*, 1947−1950.

(73) Karumbaiah, L.; Enam, S. F.; Brown, A. C.; Saxena, T.; Betancur, M. I.; Barker, T. H.; Bellamkonda, R. V. Chondroitin Sulfate Glycosaminoglycan Hydrogels Create Endogenous Niches for Neural Stem Cells. *Bioconjugate Chem.* **2015**, *26*, 2336−2349.

(74) Farrugia, B. L.; Lord, M. S.; Whitelock, J. M.; Melrose, J. Harnessing Chondroitin Sulphate in Composite Scaffolds to Direct Progenitor and Stem Cell Function for Tissue Repair. *Biomater. Sci.* **2018**, *6*, 947−957.

(75) Pomin, V. H.; Mulloy, B. Glycosaminoglycans and Proteoglycans. *Pharmaceuticals* **2018**, *11*, 27.

(76) Tian, B.; Xu, S.; Rogers, J. A.; Cestellos-Blanco, S.; Yang, P.; Carvalho-de-Souza, J. L.; Bezanilla, F.; Liu, J.; Bao, Z.; Hjort, M.; Cao, Y.; Melosh, N.; Lanzani, G.; Benfenati, F.; Galli, G.; Gygi, F.; Kautz, R.; Gorodetsky, A. A.; Kim, S. S.; Lu, T. K.; Anikeeva, P.; Cifra, M.; Krivosudský, O.; Havelka, D.; Jiang, Y. Roadmap on Semiconductor-Cell Biointerfaces. *Phys. Biol.* **2018**, *15*, 031002.

(77) Labeed, F. H.; Lu, J.; Mulhall, H. J.; Marchenko, S. A.; Hoettges, K. F.; Estrada, L. C.; Lee, A. P.; Hughes, M. P.; Flanagan, L. A. Biophysical Characteristics Reveal Neural Stem Cell Differentiation Potential. *PLoS One* **2011**, *6*, e25458.

(78) Schindelin, X. J.; Arganda-Carreras, I.; Frise, E.; Kaynig, V.; Longair, M.; Pietzsch, T.; Preibisch, S.; Rueden, C.; Saalfeld, S.; Schmid, B.; Tinevez, J. Y.; White, D. J.; Hartenstein, V.; Eliceiri, K.; Tomancak, P.; Cardona, A. Fiji: An Open-Source Platform for Biological-Image Analysis. *Nat. Methods* **2012**, *9*, 676−682.

(79) Arulmoli, J.; Wright, H. J.; Phan, D. T. T.; Sheth, U.; Que, R. A.; Botten, G. A.; Keating, M.; Botvinick, E. L.; Pathak, M. M.; Zarembinski, T. I.; Yanni, D. S.; Razorenova, O. V.; Hughes, C. C. W.; Flanagan, L. A. Combination Scaffolds of Salmon Fibrin, Hyaluronic Acid, and Laminin for Human Neural Stem Cell and Vascular Tissue Engineering. *Acta Biomater.* **2016**, *43*, 122−138.

(80) Lissner, M. M.; Thomas, B. J.; Wee, K.; Tong, A. J.; Kollmann, T. R.; Smale, S. T. Age-Related Gene Expression Differences in Monocytes from Human Neonates, Young Adults, and Older Adults. *PLoS One* **2015**, *10*, e0132061.

(81) Goecks, J.; Nekrutenko, A.; Taylor, J.; The Galaxy Team. Galaxy: A Comprehensive Approach for Supporting Accessible, Reproducible, and Transparent Computational Research in the Life Sciences. *Genome Biology* **2010**, *11*, R86.

(82) Trapnell, C.; Williams, B. A.; Pertea, G.; Mortazavi, A.; Kwan, G.; van Baren, M. J.; Salzberg, S. L.; Wold, B. J.; Pachter, L. Transcript Assembly and Quantification by RNA-Seq Reveals Unannotated Transcripts and Isoform Switching During Cell Differentiation. *Nat. Biotechnol.* **2010**, *28*, 511−515.

(83) Mortazavi, A.; Williams, B. A.; McCue, K.; Schaeffer, L.; Wold, B. Mapping and Quantifying Mammalian Transcriptomes by RNA-Seq. *Nat. Methods* **2008**, *5*, 621−628.